The Astronomical Journal, 142:71 (15pp), 2011 September doi:10.1088/0004-6256/142/3/71

A KINEMATIC AND PHOTOMETRIC STUDY OF THE GALACTIC YOUNG STAR CLUSTER NGC 7380

W. P. Chen[1,2], A. K. Pandey[3], Saurabh Sharma[3,4], C. W. Chen[1], Li Chen[5], J. Sperauskas[6], K. Ogura[7], R. J. Chuang[8], and R. P. Boyle[9]

[1] Institute of Astronomy, National Central University, Jhongli 32001, Taiwan
[2] Department of Physics, National Central University, Jhongli 32001, Taiwan
[3] Aryabhatta Research Institute of Observational Sciences, Manora Peak, Nainital 263 129, Uttaranchal, India
[4] INAF-Osservatorio Astrofisico di Arcetri, Largo E. Fermi 5, I-50125 Firenze, Italy
[5] Shanghai Astronomical Observatory, Chinese Academy of Sciences, Shanghai 200030, China
[6] Astronomical Observatory of Vilnius University, Lithuania
[7] Department for Natural Sciences, Kokugakuin University, Higashi, Shibuya-ku, Tokyo 150-8440, Japan
[8] Department of Statistics and Information Science, Fu Jen University, Taiwan
[9] Vatican Observatory Research Group, Steward Observatory, Tucson, AZ 85721, USA
Received 2010 December 5; accepted 2011 June 16; published 2011 August 9

ABSTRACT

We present proper motions, radial velocities, and a photometric study of the Galactic open cluster NGC 7380, which is associated with prominent emission nebulosity and dark molecular clouds. On the basis of the sample of highly probable member stars, the star cluster is found to be at a distance of 2.6 ± 0.4 kpc, has an age of around 4 Myr, and a physical size of ~6 pc across with a tidal structure. The binary O-type star DH Cep is a member of the cluster in its late stage of clearing the surrounding material, and may have triggered the ongoing star formation in neighboring molecular clouds which harbor young stars that are coeval and comoving with, but not gravitationally bound by, the star cluster.

Key words: open clusters and associations: individual (NGC 7380) – stars: formation – stars: luminosity function, mass function – stars: pre-main sequence

Online-only material: color figures, machine-readable and VO table

1. INTRODUCTION

The Galactic open cluster NGC 7380 (R.A. = $22^h47^m21^s$, decl. = 58°07′54″) is associated with the prominent bright nebula, recognized as early as 1787 by Caroline Herschel and later cataloged by Sharpless as S 142 (Sharpless 1959). With a large sky projected size of 25′ and richness in stellar content, the nebulosity is connected to active, ongoing star formation as evidenced by its relation to the H II region, Hα emission stars, and bright-rimmed clouds (BRCs; Ogura et al. 2002). Located within S 142 is the compact star cluster, NGC 7380, which is known to have a prominent pre-main-sequence (PMS) population (Baade 1983), and is listed in the *WEBDA* database[10] as having an age of 12 Myr. A description of the general NGC 7380 complex including the star cluster and H II region together with atomic and molecular clouds is given by Chavarria-K. et al. (1994).

Distance determinations of NGC 7380 found in the literature include ~1.43 kpc (Tadross et al. 2002, by *UBV* CCD photometry, $E_{B-V} = 0.5$), 2.4 kpc (Georgelin & Georgelin 1976), 2.82 kpc (Becker & Fenkart 1971, by *UBV* photoelectric (PE) photometry, $E_{B-V} = 0.80$), 3.2 kpc (Chavarria-K. et al. 1994, by *uvby*-β photometry, $E_{B-V} = 0.66$), and 3.6 kpc (Moffat 1971, by *UBV* photographic photometry). Such discrepancies are not unusual for a young stellar group for which patchy extinction often leads to inconsistent results when different techniques (e.g., photometry, spectroscopy) are applied to distinct stellar populations (e.g., main-sequence fitting versus massive stars). NGC 7380 is known to be associated with such a variable extinction and it has a deficit of faint stars at its center (Moffat 1971). The luminous stars in the region have been known to have a very high fraction of binarity (Underhill 1969), which may also affect the distance determinations. Moreover, many OB stars are found far outside the cluster, and may be part of the Cep OB1 association. Therefore care must be taken when determining the properties of the star cluster several arcminutes across, seen against a possibly expanding OB association with an angular extent of several degrees.

In any case, this star-forming complex appears to be in the interior of the Perseus arm, with a systemic $v_{LSR} \sim -35.8$ km s^{-1} (Georgelin & Georgelin 1976). Chavarria-K. et al. (1994) studied the general area around NGC 7380, including the star cluster itself and the H II region S 142 together with the associated, relatively compact molecular cloud NGC 7380E (Leisawitz et al. 1989), and found a good agreement between the radial velocity (RV) of the H II region (−40.3 km s^{-1}) and those of the molecular cloud (−41.2 km s^{-1}) and the star cluster (−37 km s^{-1}).

Here we present kinematic (proper motions and RV) and multiwavelength studies of the Galactic open cluster NGC 7380 in order to determine its properties and evolutionary status in relation to neighboring stars and nebulosity. Section 2 presents the data and analysis, Section 3 summarizes the results, and Section 4 discusses the star formation history and activity in the cluster.

2. DATA AND ANALYSIS

2.1. Photometric Data

CCD $UBVI_c$ observations were obtained using the 105 cm Schmidt telescope of the Kiso Observatory on 2004 November 17, 2005 November 24, and 2007 October 31. The CCD camera used an SITe TK2048E chip having 2048 × 2048 pixels. At the Schmidt focus (f/3.1) each 24 μm pixel corresponds to 1.″5,

[10] http://www.univie.ac.at/webda/

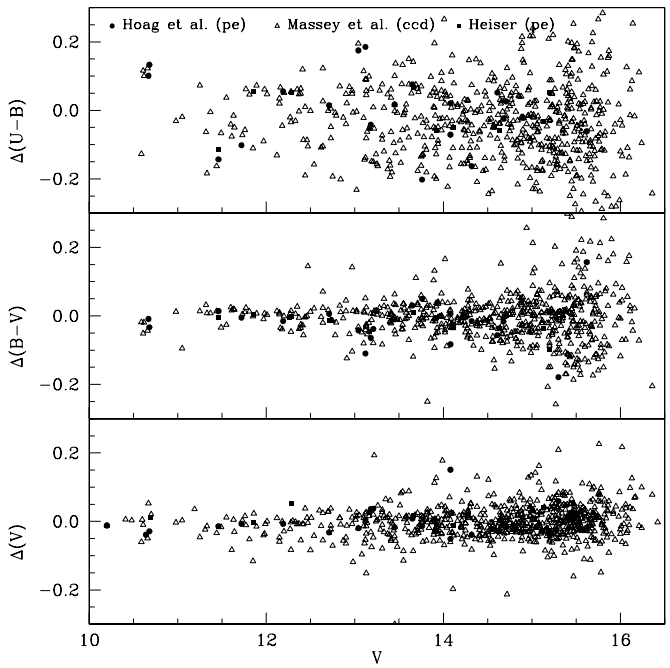

Figure 1. Comparison of present photometry data with those given in the literature. The magnitude difference (Δ = literature − present study) is plotted as a function of our *V* magnitude as the abscissa.

so the entire detector covers a field of view of $\sim 50 \times 50$ arcmin^2 on the sky. The readout noise and gain of the CCD are 23.2 e^- and 3.4 e^-/ADU, respectively. The 2004 run consisted of short- and long-exposure *UBV* frames to observe bright and faint stars in the field. The 2005 and 2007 runs took only *V* and *I* frames. For each run, the photometric SA 92 standard field (Landolt 1992) was observed, together with bias, dark, and dome-flat frames.

The CCD images were reduced using the IRAF[11] and ESO-MIDAS[12] packages. Stellar photometry was performed using DAOPHOT-II (Stetson 1987), for which the point-spread function (PSF) was obtained for each frame using several isolated stars with a good signal-to-noise ratio (S/N). For bright stars saturated on long-exposure frames, we took their magnitudes from short-exposure frames. We used the DAOGROW task to construct an aperture growth curve to correct for aperture photometry in comparison with the PSF-fitting magnitude. To estimate the incompleteness of our data, e.g., due to the flux limit of the observations, or to crowding of stars, we used the DAOPHOT II/ADDSTAR routine to inject artificial stars of random brightness at random positions into our optical images, and then processed the images in the same manner to determine the completeness of the data (Sagar & Richtler 1991; Pandey et al. 2001, 2005). The completeness factors for the cluster and for the field regions are similar and are listed in Table 2. Our optical data are about 90% complete at $V \sim 17.5$ mag.

Early photometric measurements of the NGC 7380 field include those by Hoag et al. (1961) and Hoag & Applequist (1965) with PE detectors, and more recently by Massey et al. (1995) by CCD imaging. Figure 1 compares our photometric measurements with those found in the literature, as a function of *V* magnitude, and the results are summarized in Table 1. In each case, the mean and standard deviation σ are based on *N* stars in a magnitude bin. The agreements are considered satisfactory. The CCD imaging photometry forms the basis for our optical study of the cluster parameters of NGC 7380.

Additional CCD images of NGC 7380 taken with interference filters Hα, [S II], and [O III] were obtained with the Lulin One-meter Telescope in 2008 August ([S II] and [O III]) and in 2010 September. For each run, a PI-1300B CCD camera was used, which, with a pixel scale of 0.″5, gave an 11 armin^{-2} field of view. These images were used to trace excited nebulosity, particularly in relation to the distribution of young stars.

2.2. Archival Data

Near-infrared (NIR) magnitudes for point sources around NGC 7380 have been obtained from the Two Micron All Sky Survey (2MASS; Skrutskie et al. 2006) Point Source Catalog. The 2MASS database provides photometry in the *J* (1.25 μm), *H* (1.65 μm), and K_s (2.17 μm) bands to a 10σ limiting magnitude of 15.8, 15.1, and 14.3, respectively. To assure photometric accuracy, we included in our analysis only stars with a photometric quality flag of ph-qual = AAA, which effectively gives an S/N $\geqslant$ 10 and photometric uncertainty <0.10 mag in every band.

The *Midcourse Space Experiment* (*MSX*) surveyed the Galactic plane within $|b| \leqslant 5^\circ$ in four mid-infrared bands between 8 and 21 μm at a spatial resolution of $\sim$18.″3 (Price et al. 2001). Two of these bands, *A* and *C*, with $\lambda(\Delta\lambda)$ corresponding to 8.28 (3.36) μm and 12.13 (1.71) μm include several unidentified infrared emission bands at 6.2, 7.7, 8.7, 11.3, and 12.7 μm. In the current study, the *MSX A*-band images around the cluster region were used to study the spatial distribution of warm interstellar dust.

The data from the *IRAS* survey in the four far-infrared bands (12, 25, 60, and 100 μm) were used to identify protostar candidates. X-ray data have been taken from the *XMM-Newton* Serendipitous Source Catalog (2XMM), produced by the *XMM* Survey Science Centre consortium on behalf of ESA (Watson et al. 2009). These data were used to select young star candidates in the region.

2.3. Kinematic Data

2.3.1. Proper Motion Measurements

The photographic plates archived at the Shanghai Astronomical Observatory (SHAO), taken by the 40 cm double astrograph at Sheshan Station, with a focal length of 6.9 m, were used to derive stellar proper motions. A total of 17 photographic plates, including one plate taken in 1919, one in 1935, five in 1955, five in 1960, and five in 1998, were scanned and digitized to measure the positions of stars (Zhao et al. 2006). The plates were taken with no filters and the emulsion had a spectral sensitivity close to that of a standard *B* band. With a maximum time baseline of 79 yr, this data set allows us to derive reliable stellar proper motions. A maximum likelihood algorithm can then compute the membership probability of a particular star in the field from its proper motion and position. The membership probability, however, was not used here because the star cluster occupies only a small portion in the field.

The proper motions measured by the SHAO plates are generally consistent with those listed in the Third USNO CCD Astrograph Catalog (UCAC3; Zacharias et al. 2010). Typical errors in proper motions range from 1 to 10 mas yr^{-1} for UCAC3, and <1 mas yr^{-1} for the SHAO measurements. The

[11] IRAF is distributed by the National Optical Astronomy Observatory, which is operated by the Association of Universities for Research in Astronomy, Inc., under cooperative agreement with the National Science Foundation.
[12] ESO-MIDAS is developed and maintained by the European Southern Observatory.

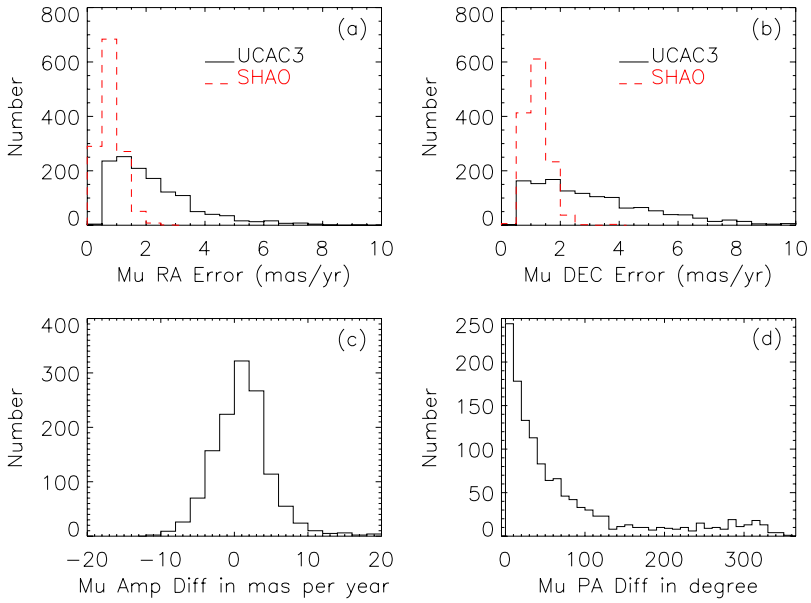

Figure 2. Comparison between the UCAC3 and SHAO measurements of a total of 1305 stars, with the proper motion errors in (a) right ascension and (b) declination, and differences in (c) amplitude and (d) position angle of the proper motion vectors. Stars with null UCAC3 error entries are not included.

(A color version of this figure is available in the online journal.)

Table 1
Comparison of the Present Photometry with the Photometry Available in the Literature, by CCD Imaging or Photoelectric (PE) Measurements

V Range	$\Delta(V)$ (Mean $\pm\sigma$)	(N)	$\Delta(B-V)$ (Mean $\pm\sigma$)	(N)	$\Delta(U-B)$ (Mean $\pm\sigma$)	(N)
			Massey et al. (1995, CCD)			
10–11	-0.005 ± 0.030	10	-0.024 ± 0.022	5	0.036 ± 0.099	5
11–12	-0.020 ± 0.035	21	0.003 ± 0.027	20	-0.033 ± 0.073	20
12–13	-0.015 ± 0.036	43	-0.003 ± 0.047	45	-0.009 ± 0.075	44
13–14	-0.004 ± 0.048	121	-0.001 ± 0.040	108	-0.025 ± 0.096	104
14–15	-0.001 ± 0.042	192	-0.012 ± 0.048	168	-0.023 ± 0.082	165
15–16	0.003 ± 0.047	274	-0.010 ± 0.079	223	-0.035 ± 0.095	200
16–17	0.022 ± 0.051	23	0.024 ± 0.078	13	-0.029 ± 0.102	12
			Heiser (1978, PE)[a]			
11–12	-0.008 ± 0.006	2	-0.002 ± 0.005	2	-0.029 ± 0.085	2
12–13	0.009 ± 0.042	2	-0.006 ± 0.006	3	0.033 ± 0.018	2
13–14	0.012 ± 0.015	3	-0.012 ± 0.023	3	-0.015 ± 0.057	3
14–15	-0.005 ± 0.007	2	-0.030 ± 0.006	2	-0.055 ± 0.004	2
15–16	0.001 ± 0.041	2	-0.069 ± 0.031	2	0.010 ± 0.042	2
			Hoag et al. (1961, PE)			
10–11	-0.027 ± 0.011	3	-0.021 ± 0.012	2	0.117 ± 0.016	2
11–12	-0.011 ± 0.004	2	0.005 ± 0.008	2	-0.122 ± 0.020	2
12–13	-0.020 ± 0.013	2	-0.005 ± 0.011	2	0.035 ± 0.020	2
13–14	0.005 ± 0.022	7	-0.026 ± 0.051	7	0.082 ± 0.088	5
14–15	0.001 ± 0.068	8	-0.027 ± 0.031	6	-0.026 ± 0.073	6
15–16	0.021 ± 0.039	2	-0.011 ± 0.168	2	$-0.061 \pm -$	1

Notes. The difference Δ (literature−present data) is in magnitude. Mean and σ are based on N stars in a V magnitude bin.
[a] Data taken from WEBDA, referenced to A. M. Heiser (1978, private communication).

proper motion vectors in general differ by less than 4 mas yr^{-1} in amplitude, and less than 30° in position angle between the two data sets (Figure 2). We downloaded the UCAC3 data from the NOMAD interface.[13] The NOMAD catalog combines various astrometric and photometric data sets. For bright stars, for example, the proper motion values by *Hipparcos* or *Tycho* might be used instead of UCAC3. For consistency, we used the UCAC3 and not the NOMAD values except in a few cases. Table 3 lists the 498 stars within a field of ∼50′ across used in this study. Columns 1 and 2 give the coordinates of the star, and Columns 3 and 4 give the SHAO and UCAC3 proper-motion measurements and associated errors. The next columns list the optical photometry measured by us and 2MASS *JHK* magnitudes. The complete table is available online.[14] We cross-referenced both SHAO and UCAC3 data sets to identify kinematic candidate members of the cluster.

[13] http://www.nofs.navy.mil/nomad.html

[14] http://www.astro.ncu.edu.tw/∼wchen/wp_chen/ngc7380pm.txt

Table 2
Completeness Factor in the Cluster and Field Regions

V Magnitude Range	NGC 7380 Region	Comparison Field
09.5–10.5	1.00	1.00
10.5–11.5	1.00	1.00
11.5–12.5	1.00	1.00
12.5–13.5	1.00	1.00
13.5–14.5	1.00	1.00
14.5–15.5	0.97	0.98
15.5–16.5	0.95	0.93
16.5–17.5	0.87	0.89
17.5–18.5	0.84	0.88
18.5–19.5	0.79	0.77

2.3.2. Radial Velocity Measurements

A selected sample of stars toward NGC 7380 were observed in 2003 and 2006 with the Coravel-type spectrometer of the Vilnius University Observatory (Upgren et al. 2002), mounted on the 1.6 m and 2.3 m telescopes at the Steward Observatory. RV measurements were collected for 15 stars, with a typical error of 0.7 km s^{-1}, at two or three epochs. The RV data provide a kinematic diagnosis of possible cluster membership in addition to proper motions. Measurements at different epochs, furthermore, would reveal RV variations caused by binary orbits. Recognition of such binary systems so as to avoid them in the main-sequence fitting is crucial when deriving parameters of a star cluster. We note that Underhill (1969) found a very high fraction of binaries in the region, with 6 detected and 4 suspected spectroscopic binaries out of 10 stars observed.

Table 4 lists the RV measurements, together with the SHAO and UCAC3 proper motions. Columns 1–4 give the identification number used in the WEBDA database, the coordinates of the star, and its angular distance of the star from the cluster center. Columns 5 and 6 list the epoch of each RV measurement, its value, and the estimated error given in parentheses. All the RV measurements were acquired by the Coravel-type spectrometer except that for DH Cep, for which the RV value was taken from Penny et al. (1997). Proper motions by SHAO and by UCAC3 are summarized in the next four columns of the table. One immediately notices from the table the necessity of acquiring six-dimensional spatial and kinematic information that is as complete as possible to determine reliable stellar membership in a star cluster. For example, Star 17, with a position well within the cluster boundary, is possibly associated with DH Cep, i.e., a member of NGC 7380, on the basis of its proper motion, but not according to its RV. Star 160, with a position far from the cluster, on the other hand, has an RV close to that of DH Cep, but the same is not true for its proper motion. Three stars, *WEBDA* 19, 160, and 1252, exhibit clear RV variations, hence should be spectroscopic binaries. Stars 19 and 1252 are within the cluster boundary, but Star 160 is far away from the cluster, so is most likely not a member of NGC 7380. This sample adds to the already rich binary inventory among the OB stars in the region. The spatial distribution of stars with both RV and proper motions available is shown in Figure 3.

3. CHARACTERIZATION OF THE CLUSTER

Our study focused on the region containing DH Cep = HD 215835 (R.A. = 22:46:54.11, decl. = +58:05:03.5, J2000), which is considered to be the primary exciting star for the H II region S 142. The star is a double-lined spectroscopic and eclipsing binary consisting of two very luminous O 5/6 stars (Hilditch et al. 1996) close to the zero-age main sequence (ZAMS). The binary is an X-ray source, perhaps attributed to colliding winds (Pittard & Stevens 2002; Bhatt et al. 2010). Our kinematic study of NGC 7380 relies on the assumption that DH Cep is a member of the cluster. DH Cep has a measured proper motion of $(\mu_\alpha, \mu_\delta) = (-1.74 \pm 0.84, -2.52 \pm 0.81)$ mas yr^{-1} (Baumgardt et al. 2000), as measured by *Hipparcos* (Perryman et al. 1997), compared with the SHAO values of $(-4.11 \pm 1.29, -2.80 \pm 1.19)$, and the UCAC3 values of $(-2.7, -3.6)$. The measured RV of DH Cep has been recorded as -33 ± 2 km s^{-1} (Hilditch et al. 1996), -35.4 ± 1.8 km s^{-1} (Pearce 1949), and -39 ± 3 km s^{-1} (Sturm & Simon 1994; Penny et al. 1997), which is consistent with it being part of the Perseus arm (Georgelin & Georgelin 1976).

Figure 4 shows the UCAC3 proper motions of stars in the ~1 deg field toward NGC 7380. The two prominent parallel arrows to the southwest of the cluster are for the known common proper-motion pair, HD 215714 and HD 240051. The pair has a heliocentric distance of less than 70 pc, as inferred from the stellar brightness and spectral type, and an RV of 6 km s^{-1} (Nordström et al. 2004), so is not associated with NGC 7380. Stars with proper motions close to that of DH Cep, marked by circles, are found to concentrate spatially, viz., the NGC 7380 cluster. Additional stars kinematically associated with DH Cep are distributed throughout the field. These should be mostly early-type stars, as judged by their 2MASS colors (Figure 5). DH Cep hence is clearly a part of NGC 7380, which in turn is associated with the surrounding OB association. The sample of kinematic members was used in the determination of cluster parameters.

3.1. Morphology and Size of the Cluster

NGC 7380 is clearly seen as a density enhancement in the surface density map of 2MASS stars (Figure 6). The cluster

Table 3
Proper Motions and Photometry of Stars near NGC 7380

R.A. (2000) (h m s)	Decl. (2000) (° ′ ″)	$\mu_\alpha\Delta\mu_\alpha\mu_\delta\Delta\mu_\delta$ (SHAO) (mas yr^{-1})	$\mu_\alpha\Delta\mu_\alpha\mu_\delta\Delta\mu_\delta$ (UCAC3) (mas yr^{-1})	*B* (mag)	*V* − *I* (mag)	*U* − *B* (mag)	*B* − *V* (mag)	*J* (mag)	*H* (mag)	*K* (mag)
22 44 56.81	+58 7 5.2	−6.450 0.755−0.999 1.383	−6.5 2.6−4.8 2.9	13.120	1.777	1.828	1.652	10.017	9.249	9.035
22 44 56.94	+58 11 9.0	+3.952 1.542−4.769 2.025	+7.0 5.3 +3.0 3.2	14.359	1.019	0.535	0.792	12.667	12.312	12.267
22 44 58.02	+57 54 27.2	−0.407 1.014−2.096 1.564	−5.1 1.7−6.6 3.6	14.214	0.607	0.550	0.490	13.138	12.979	12.940
22 44 58.37	+58 21 44.5	−1.215 0.334−1.026 0.863	−2.9 0.7−1.8 0.8	12.171	0.615	1.248	0.460	11.141	11.056	10.950
22 45 0.04	+58 11 32.4	−0.451 0.624−3.520 1.096	−4.2 1.1−4.4 2.0	12.945	0.643	0.557	0.488	11.809	11.718	11.618

(This table is available in its entirety in machine-readable and Virtual Observatory (VO) forms in the online journal. A portion is shown here for guidance regarding its form and content.)

Table 4
Kinematics of Stars toward NGC 7380

WEBDA No.	R.A. (2000) Decl. (2000) (h m s °′″)	Ang. (arcmin)	JD (+2400000)	RV (km s^{-1})	mu_α, μ_δ (SHAO) (mas yr^{-1})	μ_α, μ_δ (UCAC3) (mas yr^{-1})
DH Cep	22 46 54.11 +58 05 03.5	1.8	...	-36 ± 3	−4.11 (1.29), −2.80 (1.19)	−2.7, −3.6
0052	22 46 16.56 +58 08 38.8	4.4	52978.605	−51.7 (0.8)	1.54 (0.96), 7.03 (1.87)	+3.8 (2.1), 0.3 (4.8)
			52998.672	−53.3 (1.1)		
			54076.678	−53.0 (0.6)		
0030	22 46 19.62 +58 11 03.6	5.8	52939.738	2.9 (0.6)	6.91 (0.71), 2.82 (0.78)	10.4 (0.7), 3.7 (0.9)
			52977.660	3.5 (0.7)		
			54082.659	3.7 (0.4)		
0056	22 46 41.42 +58 08 02.0	2.6	52978.617	−57.6 (0.8)		−8.0 (1.6), −5.8 (2.6)
			52998.648	−58.1 (1.1)		
			54076.728	−56.5 (0.8)		
0048	22 46 42.54 +58 08 05.2	2.6	52977.703	−20.4 (0.7)	6.87 (0.68), −3.59 (1.86)	4.3 (1.9), −1.7 (6.8)
			52998.633	−19.5 (0.8)		
			54076.702	−20.9 (0.5)		
0065	22 46 46.82 +58 04 23.4	2.7	52978.652	−76.7 (0.9)		−3.9 −13.8
			54083.744	−77.6 (0.9)		
1252	22 46 52.74 +58 08 36.2	2.6	52939.727	−63.2 (0.7)	−3.46 (0.96), −10.11 (1.53)	0.0 (5.2), −9.0 (6.4)
			52977.669	−60.5 (0.7)		
			54082.682	−66.9 (0.5)		
0017	22 47 20.67 +58 07 50.7	1.5	52977.723	−70.2 (0.9)	3.00 (0.92), 1.06 (1.67)	−0.3 (1.9), −3.6 (4.3)
			53000.626	−67.8 (1.5)		
			54082.734	−73.3 (0.4)		
1203	22 47 20.90 +58 13 17.9	6.9	52939.801	−25.5 (0.8)	−0.65 (1.25), −4.60 (1.67)	−2.4 (1.5), 1.9 (6.1)
			52977.741	−27.3 (0.9)		
			54082.720	−24.8 (0.6)		
0014	22 47 29.91 +58 05 58.0	1.2	52939.770	−27.8 (0.7)	−2.20 (1.21), −4.85 (0.74)	3.4 (3.0), 0.3 (10.2)
			52980.635	−28.0 (0.7)		
			54083.706	−26.8 (0.6)		
0160	22 47 35.63 +58 17 55.8	11.6	52939.746	−38.9 (0.7)	23.05 (0.31), −0.59 (1.25)	24.3 (1.4), −2.2 (1.4)
			52977.688	−39.3 (0.7)		
			54082.669	−32.0 (0.5)		
0019	22 47 37.08 +58 03 49.8	3.0	52980.692	−68.2 (1.5)	−12.95 (1.06), −5.36 (1.68)	−15.2 (1.4), −9.2 (4.5)
			54083.727	−44.3 (1.1)		
0043	22 47 59.68 +58 08 28.6	3.7	52939.695	−33.6 (0.7)	2.39 (0.73), −3.80 (1.58)	−1.6 (2.0), −0.7 (1.8)
			52980.650	−34.3 (0.7)		
			54082.692	−34.2 (0.5)		
0171	22 48 14.58 +58 12 32.6	7.4	52939.688	−32.4 (0.6)	−4.71 (0.74), −1.71 (1.40)	0.2 (1.8), −6.6 (2.4)
			52980.660	−32.2 (0.6)		
			54082.664	−31.8 (0.4)		
0172	22 48 50.89 +58 15 35.6	11.3	52939.707	−33.5 (0.7)	−3.59 (0.62), 0.78 (1.07)	−4.4 (2.0), −1.6 (2.0)
			54082.674	−32.6 (0.5)		
5716	22 49 58.31 +58 11 52.5	12.3	52939.758	−49.7 (0.7)	1.14 (0.63), −1.47 (0.85)	+0.7 (2.5), +1.9 (4.0)
			52977.678	−49.6 (0.7)		
			54082.706	−49.9 (0.4)		

is elongated in the north–south direction, with an average angular size of 3′–5′. In addition, there is an extension of stellar distribution to the west, i.e., in the opposite direction of the dark cloud NGC 7380E and the ionized gas located immediately to the east and southeast of—hence encompassing—the cluster. Given the somewhat irregular shape, the "center" of the star cluster was visually determined, to be at R.A. = $22^{\rm h}47^{\rm m}13^{\rm s}$ and decl. = +58°06′25″(J2000). Note DH Cep is to a side of the cluster, opposite the molecular cloud. The proper motions (Figure 4) also suggest a spatial grouping of 3′–4′ in radius. Kharchenko et al. (2005) determined a 6′ radius for the core, and 9′ for the corona, of NGC 7380, with a sample of eight probable member stars (proper motions and main sequence) brighter than $m_V \sim 14$ mag. Our size determination agrees with the core size considering the extended shape and if the tail to the west is included. Henceforth we refer to a 4′ radius around this center as the "cluster region," shown in Figure 3.

3.2. Interstellar Extinction and Reddening

The interstellar extinction in the cluster region is estimated using the $(U - B)$ versus $(B - V)$ color–color diagram, or the two-color diagram (TCD) shown in Figure 7. The reddening for every star with a photometric uncertainty less than 0.1 mag, and with a spectral type earlier than A0, has been derived using the Q method (Johnson & Morgan 1953; Jose et al. 2008, 2011), and suggests a generally lower reddening in the cluster region than in the outer region (Figure 8). The two maxima near 7′ and 15′ had previously been identified as "dust shells" (Moffat 1971).

To investigate the nature of the reddening law, we used the $(V - \lambda)$ versus $(B - V)$ TCDs to distinguish normal extinction produced by grains in the diffuse interstellar medium from that caused by abnormal dust grains (Chini & Wargau 1990; Pandey et al. 2000). Here λ is the wavelength of one of the broadband

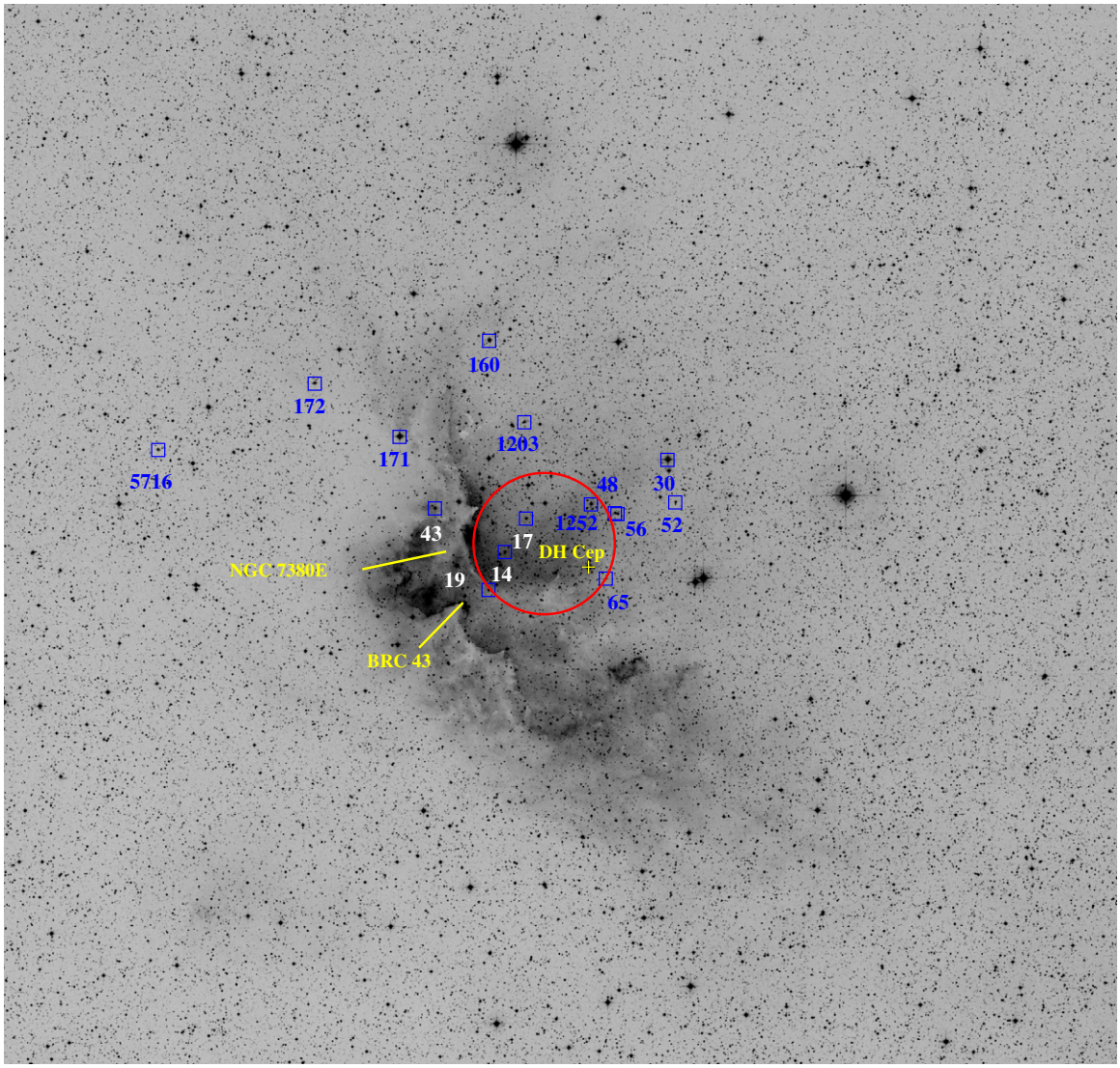

Figure 3. Stars with both RV and proper motion measured (listed in Table 4) are denoted by squares and labeled with the *WEBDA* numbers on a DSS R2 image. The bright-rimmed cloud BRC 43, the molecular cloud NGC 7380E, and the O-type star DH Cep (marked by a cross) are labeled. The cluster region of NGC 7380 is encircled. The field is about 50′ on a side, with north to the top and east to the left.

(A color version of this figure is available in the online journal.)

filters R, I, J, H, K, or L. We found the $E(V-\lambda)/E(B-V)$ values to be comparable to the normal values, consistent with what was reported by Chavarria-K. et al. (1994). We therefore adopted a normal reddening law, i.e., $R_V = 3.1$, for NGC 7380.

3.3. Distance and Age of the Cluster

Figure 9 shows the molecular cloud traced by CO ($J = 1$–0) emission (Leisawitz et al. 1989) of the region, superimposed on the Digital Sky Survey (DSS) red image. The cluster is clearly embraced by dark clouds, which is also evidenced in the star-count map of Figure 6. A comparison is made between the stellar population in the cluster, marked as the circle labeled "C," and that in a reference field, marked as the circle labeled "F." In the V versus $(V-I)$ color–magnitude diagram (CMD) for the cluster region (Figure 10(a)), contamination by field stars is clearly visible. Some of these could be massive stars belonging to the background Norma–Cygnus (outer) arm population (Carraro et al. 2005; Pandey et al. 2006). To remove contamination from field stars, we statistically subtracted their contribution from the cluster CMD using the following procedure. The CMD is divided by grids of $V = 1$ mag and $(V-I) = 0.4$ mag in width. The number of stars in the cluster CMD and in the field CMD is counted, respectively, within each corresponding grid cell, and after applying the completeness correction (as discussed in Section 2.1) to both samples, the number of field stars to be removed is determined. Within a grid cell, then, for each star in the field CMD (Figure 10(b)), the nearest star in the cluster CMD within $V \pm 0.25$ and $(V-I) \pm 0.125$ of the field star would be removed. The statistically cleaned cluster CMD is shown in Figure 11; the presence of PMS stars is obvious.

The statistically cleaned V versus $(V-I)$ CMD shown in Figure 11 is overlaid with a 4 Myr main sequence (Bertelli et al. 1994) and PMS isochrones (Siess et al. 2000) for various stellar masses and ages. One sees a PMS population with an age spread of mainly 1–5 Myr. Using $E(B-V) = 0.5$, $A_V = 3.1\,E(B-V)$, and $E(V-I) = 1.25\,E(B-V)$, we visually fit the theoretical isochrone according to Bertelli et al. (1994) for an age of 4 Myr and $Z = 0.02$ to the upper main sequence, and found a distance modulus $(m-M)_V = 13.60 \pm 0.35$ corresponding to a distance of 2.6 ± 0.4 kpc. The same

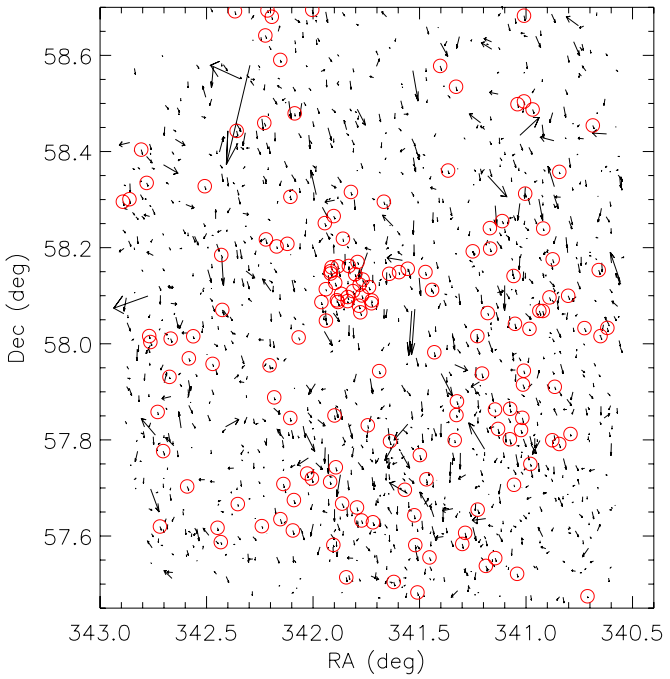

Figure 4. UCAC3 proper motions of stars in the ∼1° field around NGC 7380, each represented by an arrow for the annual angular speed and direction. Marked in circles are stars with an angular speed within 2 mas yr^{-1} and a position angle within 10° of DH Cep. Note the apparent paucity of member stars at the center of the cluster, seen near the middle of the figure.

(A color version of this figure is available in the online journal.)

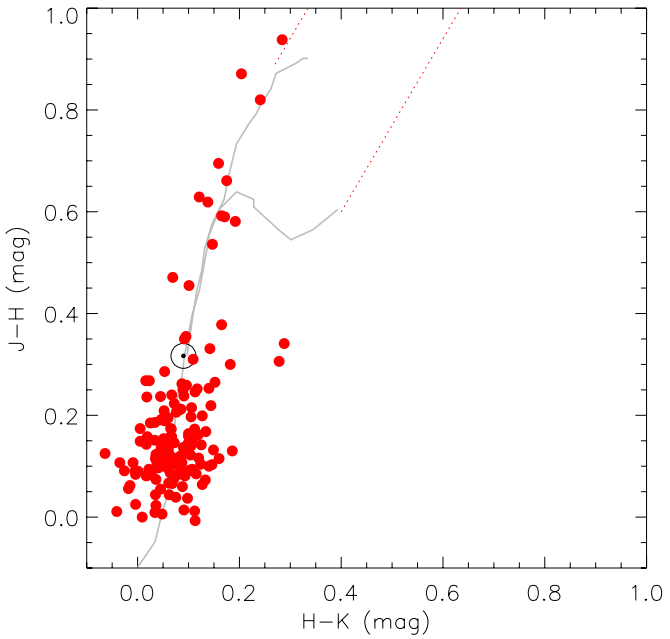

Figure 5. 2MASS $J-H$ vs. $H-Ks$ colors of the kinematically associated stars, i.e., those shown with a circle in Figure 4. The loci for dwarfs and giants (gray curves, earlier spectral types to the lower left) are from Bessell & Brett (1988), along with the reddening vector (dotted lines) by Cohen et al. (1981). Stars near the 2MASS sensitivity limit cause scattering of the data, but the majority of stars have 2MASS colors of early-type stars. The Sun is marked with the ⊙ symbol.

(A color version of this figure is available in the online journal.)

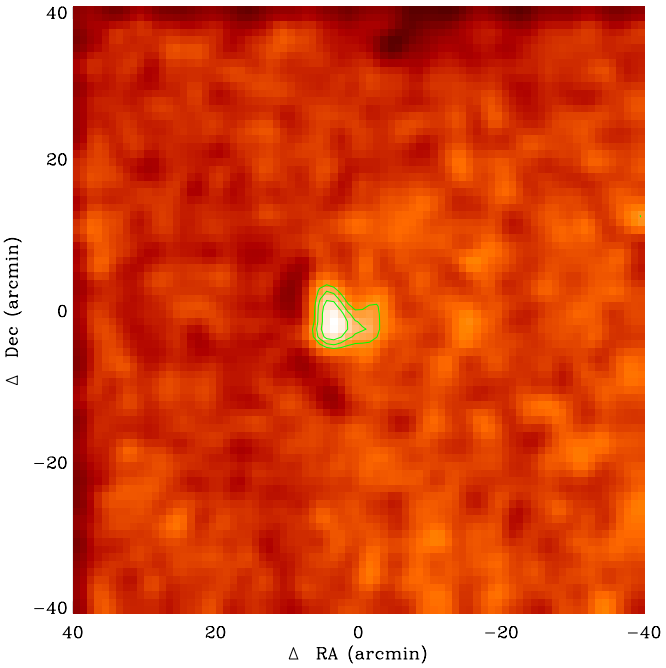

Figure 6. Isodensity contours of stars in the 2MASS K_s band. The innermost contour is for 5σ above the background surface number density, and is approximated by an ellipse with major and minor axes of 2.′66 and 1.′83, respectively, i.e., with an aspect ratio of 0.69. The outermost contour is for 3σ and is represented by an ellipse with major and minor axes of 5.′29 and 3.′85, respectively, thus with an aspect ratio of 0.73. The stellar distribution is elongated in the equatorial north–south direction, with an extension to the west.

(A color version of this figure is available in the online journal.)

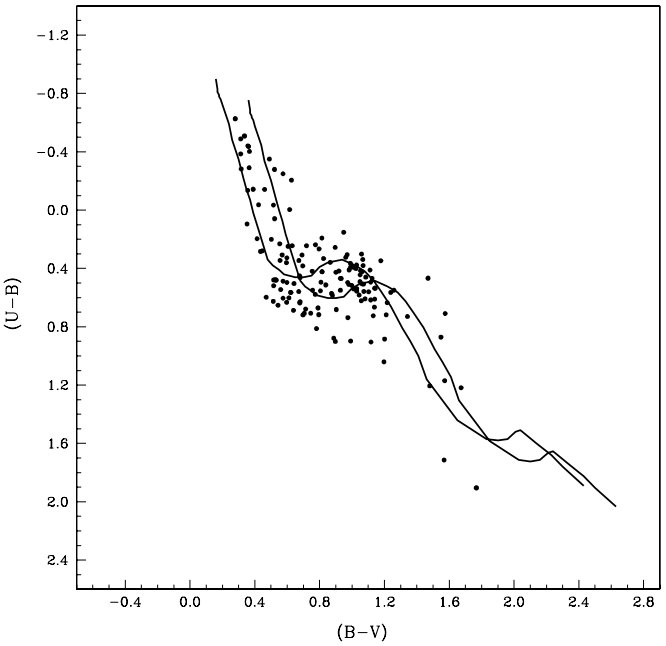

Figure 7. $(U-B)$ vs. $(B-V)$ TCD for the stars seen in the cluster. The two continuous curves represent the ZAMS (Schmidt-Kaler 1982) shifted along the reddening vector with a slope of $E(U-B)/E(B-V) = 0.72$ by $E(B-V)_{\rm min} = 0.5$ and $E(B-V)_{\rm max} = 0.7$, respectively.

consistent set of age and distance is obtained when stars known to have a spectral type earlier than A0 in the cluster region were dereddened individually using the Q method (Figure 12). At a distance of 2.6 kpc, the angular radius of the cluster, ∼4′, corresponds to a physical size of 6 pc across.

Figure 13 shows the J versus $(J-K)$ diagram for all the 2MASS sources in the field. Using 20 probable member stars based on V versus $(B-V)$ photometry and *Tycho-2* proper

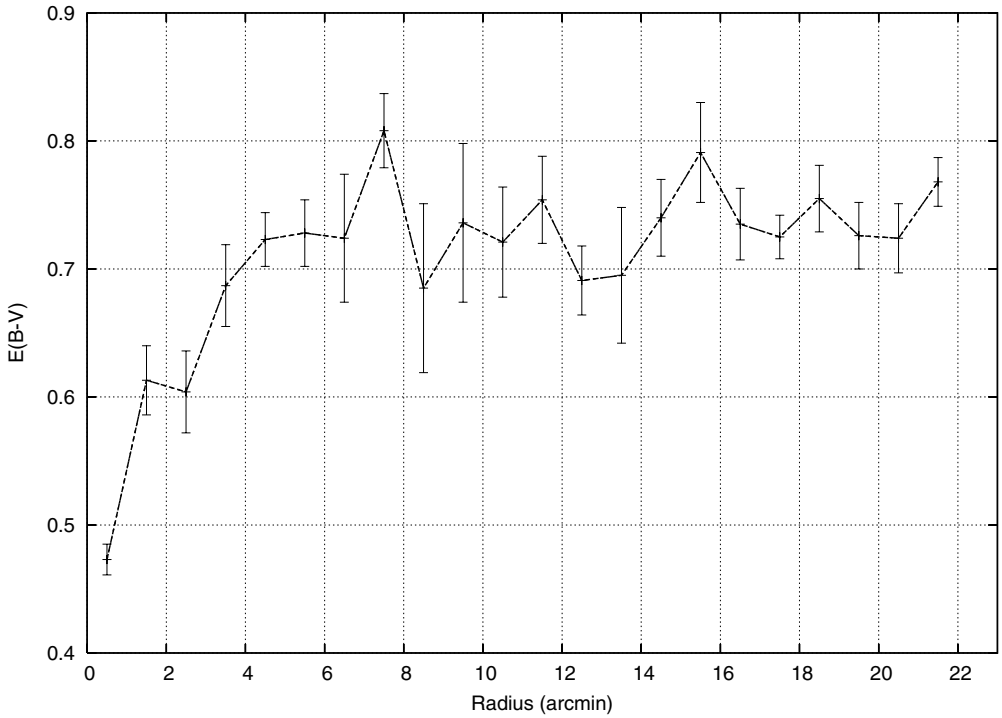

Figure 8. Spatial variation of reddening from the cluster center outward. Error bars represent standard errors.

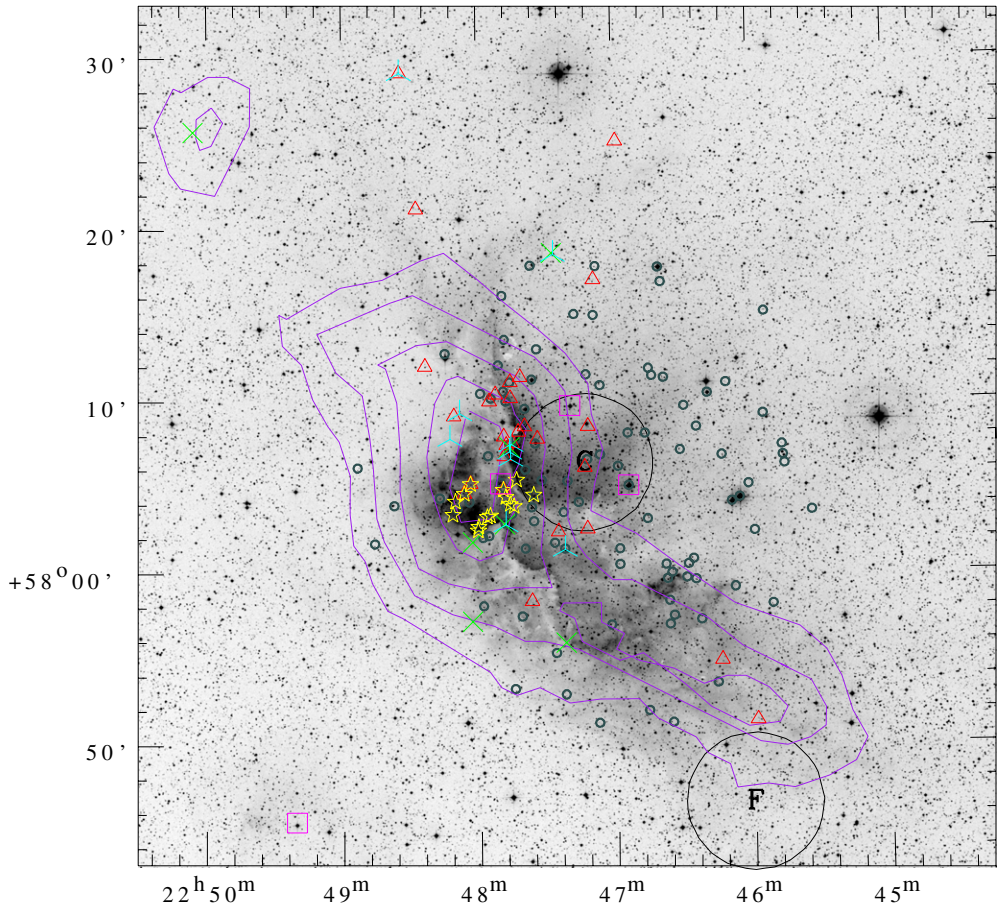

Figure 9. Spatial distributions of IR-excess sources (probable T-Tauri-type stars, open triangles), $H\alpha$ stars (stars), *IRAS* point sources (crosses), *MSX* point sources (three-pointed stars), O-type stars (open squares), and X-ray stars (open circles) are overlaid on the DSS-2 *R*-band $50' \times 50'$ image. The abscissa and the ordinates are for the J2000 epoch. The CO contours (Leisawitz et al. 1989) are overlaid. The cluster and field regions are each represented by a circle marked by "C" and "F," respectively.

(A color version of this figure is available in the online journal.)

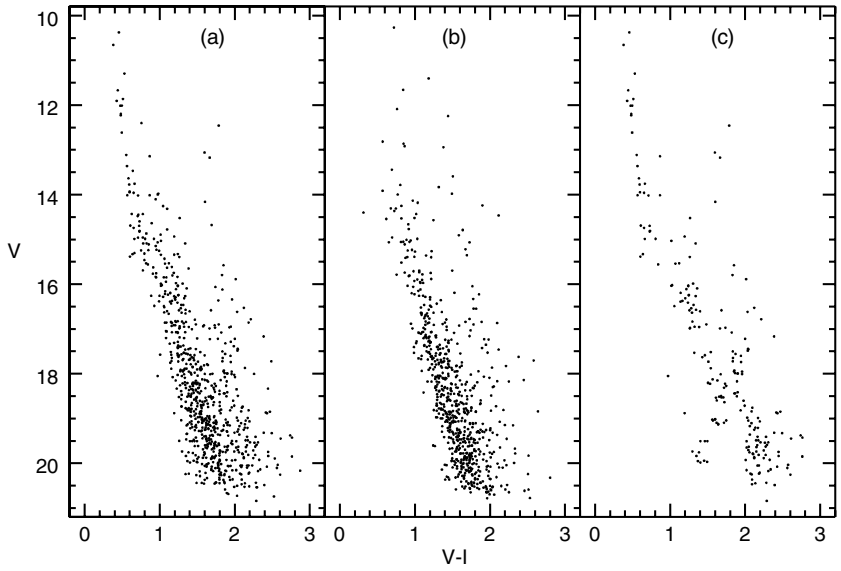

Figure 10. V vs. $(V - I)$ CMD for stars (a) in the cluster region and (b) in the field region.

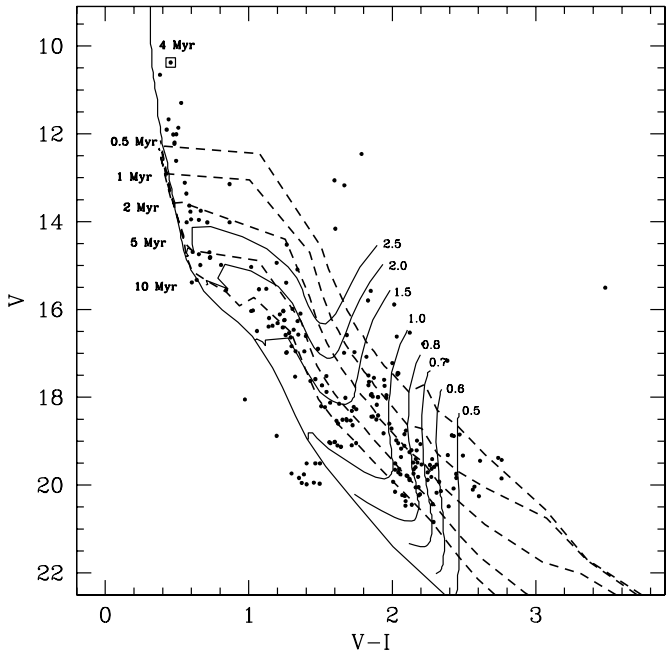

Figure 11. Statistically cleaned V vs. $(V - I)$ CMD for stars lying in the cluster region. The 4 Myr main sequence by Bertelli et al. (1994) and PMS isochrones of 0.5, 1, 2, 5, and 10 Myr along with evolutionary tracks for different stellar masses (Siess et al. 2000) are also shown. A distance of 2.57 kpc and $E(B - V) = 0.5$ mag have been assumed. The square marks DH Cep.

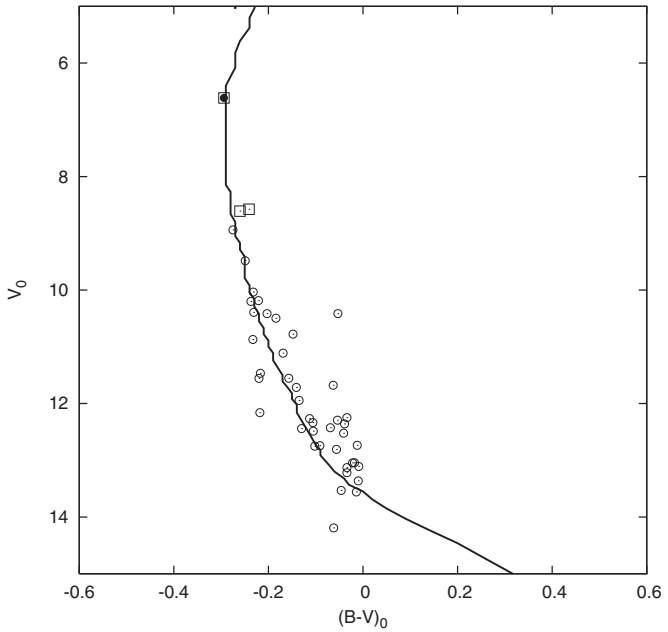

Figure 12. Dereddened CMD for stars known to have a spectral type earlier than A0 seen in the cluster region. The isochrone by Bertelli et al. (1994) for solar metallicity and age = 4 Myr is plotted for a distance of 2.57 kpc. Squares represent O-type stars. The data for DH Cep were taken from Hoag et al. (1961).

motions, Loktin & Beshenov (2003) derived the mean proper motion of the cluster as $(-2.77 \pm 0.50, -3.55 \pm 0.58)$ mas yr^{-1}, which is essentially that for DH Cep. We followed the same exercise and selected member stars photometrically and kinematically, i.e., stars projected within the cluster boundary and with proper motions within 2 mas yr^{-1} of that of DH Cep. These stars are consistent with a 4 Myr upper main sequence and with the presence of PMS stars (Figure 13).

3.4. Stellar Population of the Cluster and Surrounding Region

Typically young stellar objects (YSOs) are recognized by their Hα emission, NIR excess, or X-ray emission. Ogura et al. (2002) identified a dozen or so T-Tauri star candidates, based on their Hα emission spectra, but their sample covered a very small area limited to the vicinity of BRC 43. Therefore, we attempted to enlarge the YSO sample by including NIR-excess and X-ray stars.

The NIR-excess sources were identified using the $(J - H)$ versus $(H - K)$ colors. Figure 14 shows the TCDs for the cluster region and the reference field. All 2MASS magnitudes—including the dwarf and giant loci—have been converted to the CIT system. We classified sources into three regions in the TCD: sources in the "F" region are considered main-sequence stars, giant stars, or Class III/Class II sources with little NIR excess. "T" sources are classical T-Tauri stars (CTTS; Class II objects) with noticeable NIR excess. The "P" sources are

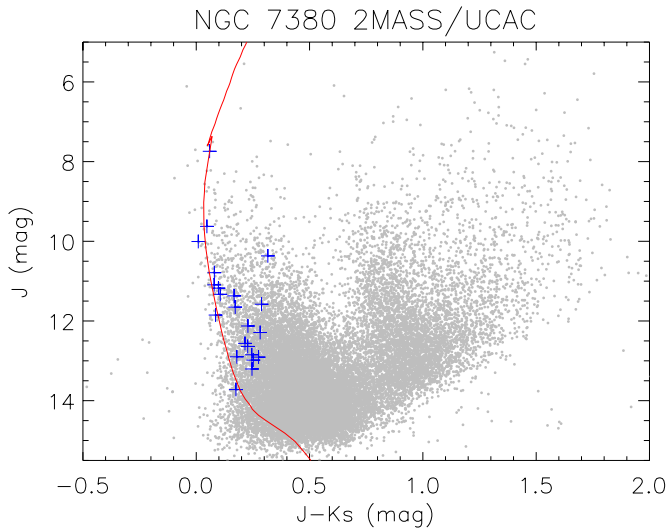

Figure 13. 2MASS J vs. $(J-K)$ diagram for all the sources (black dots) within 2° of the NGC 7380 field. Crosses mark probable kinematic member stars, chosen as being (1) spatially within 5′ of the cluster center, (2) kinematically within 2 mas yr^{-1} of the proper motion of DH Cep, and (3) $J < 15$ mag, $H < 14$ mag, and $K < 14$ mag. The solid line represents the 4 Myr main sequence (Bertelli et al. 1994) at 2.57 kpc, shifted by an extinction of $A_J = 0.282\,A_V$ and a reddening of $A_J - A_K = 0.17\,A_V$, assuming $A_V = 1.5$ mag. The upper main sequence fits reasonably well to the luminous members, whereas less massive members are still in the PMS phase.

(A color version of this figure is available in the online journal.)

either extragalactic sources or, when seen against a star-forming region, Class I objects or protostar-like objects. It is not surprising that such a classification on the basis of 2MASS colors alone is not unambiguous; there may be overlaps between T-Tauri and Herbig Ae/Be populations (Hillenbrand et al. 1992), or between T-Tauri stars and protostars (Robitaille et al. 2006). A few sources located within the cluster boundary and having colors in the "T" region in the CMD are CTTS candidates. Stars within the cluster boundary, lying in the "F" region in the CMD, but above the extension of the CTTS locus, may be weak-lined T-Tauri star (WTTS) candidates or reddened field giant stars.

We now examine the YSOs in the entire region. Figure 15 plots the $(J-H)$ versus $(H-K)$ TCD and J versus $(J-H)$ CMD for the Hα stars, X-ray stars, O-type stars, CTTSs, and WTTSs identified in Figure 14 in the entire field, i.e., within and beyond the cluster region. These YSO candidates have a very young age, less than 5 Myr, as inferred by the isochrones in the NIR CMD, and also by the optical CMD (Figure 16). Note how Figure 16 resembles that of the statistically cleaned CMD of the cluster region (see Figure 11).

3.5. Initial Mass Function and K-band Luminosity Function

With the statistically cleaned CMD (Figure 11), we are now ready to derive the mass function of the cluster using the theoretical evolutionary model. We included only stars younger than 10 Myr. With an age of ∼4 Myr for NGC 7380, a star having $V < 14$ mag ($V_0 < 12.5$; $M > 3.5\ M_\odot$) should be on the main sequence, whose mass was inferred by its luminosity using theoretical models (Bertelli et al. 1994). Otherwise the stellar mass was estimated by PMS tracks (Siess et al. 2000). The mass function, obtained by counting the number of stars in mass bins in the mass range $1.0 < M/M_\odot < 16.4$, has a slope of -1.27 ± 0.10 (Figure 17), similar to the nominal value of -1.35 for the field population in the solar neighborhood (Salpeter 1955), though there seems to be a lack of stars at the lower mass end, $M \sim 1\ M_\odot$, of our sample.

We next derive the infrared K-band luminosity function (KLF) of the cluster. To do this, our data need to be corrected for incompleteness and field star contamination. For

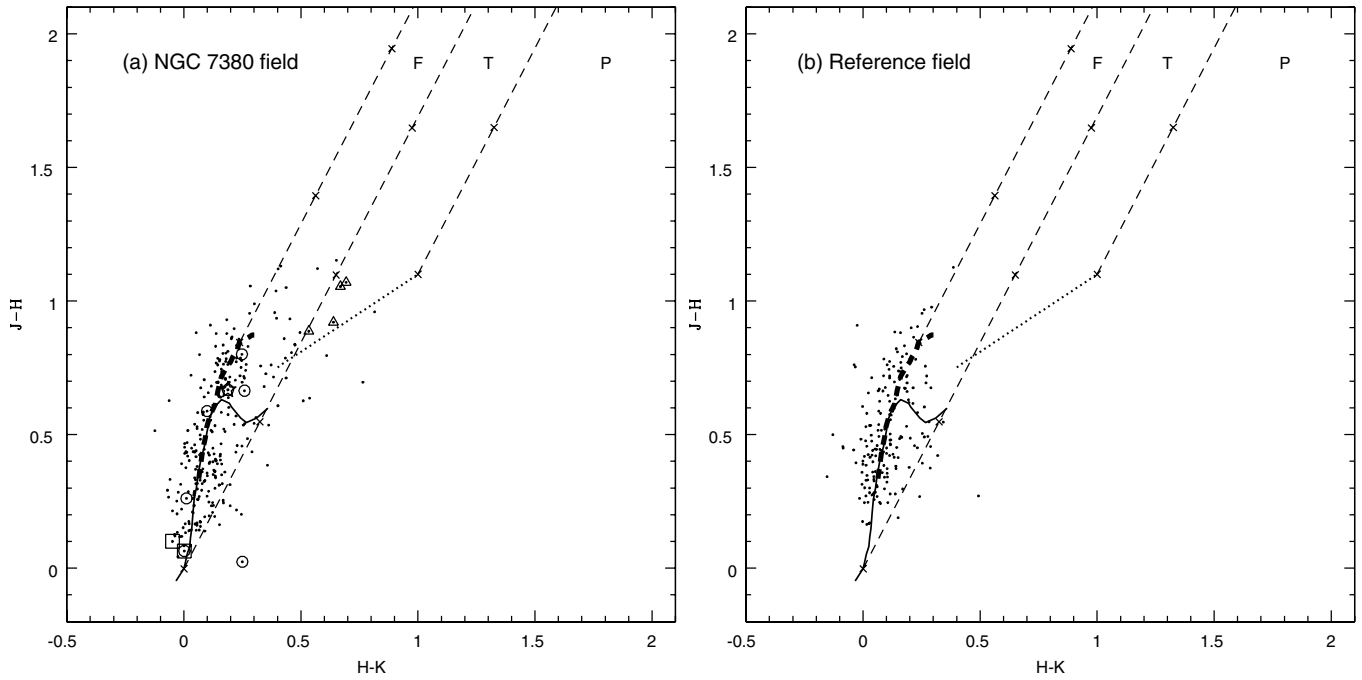

Figure 14. $(J-H)$ vs. $(H-K)$ diagram of sources (a) in the cluster and (b) in the reference field. Only stars with JHK_s photometric errors less than 0.1 mag are shown. The loci for dwarfs (solid curve) and giants (thick dashed curve) are from Bessell & Brett (1988), whereas the dotted line represents the locus of unreddened CTTSs (Meyer et al. 1997), and the dashed lines are the reddening vectors drawn from the base and tip of the two loci, adopting $A_J/A_V = 0.265$, $A_H/A_V = 0.155$, and $A_K/A_V = 0.090$ (Cohen et al. 1981), with each cross indicating an increment of $A_V = 5$ mag. Marked in the cluster region are known YSOs, O-type stars (squares), X-ray (circles), and NIR-excess sources (triangles).

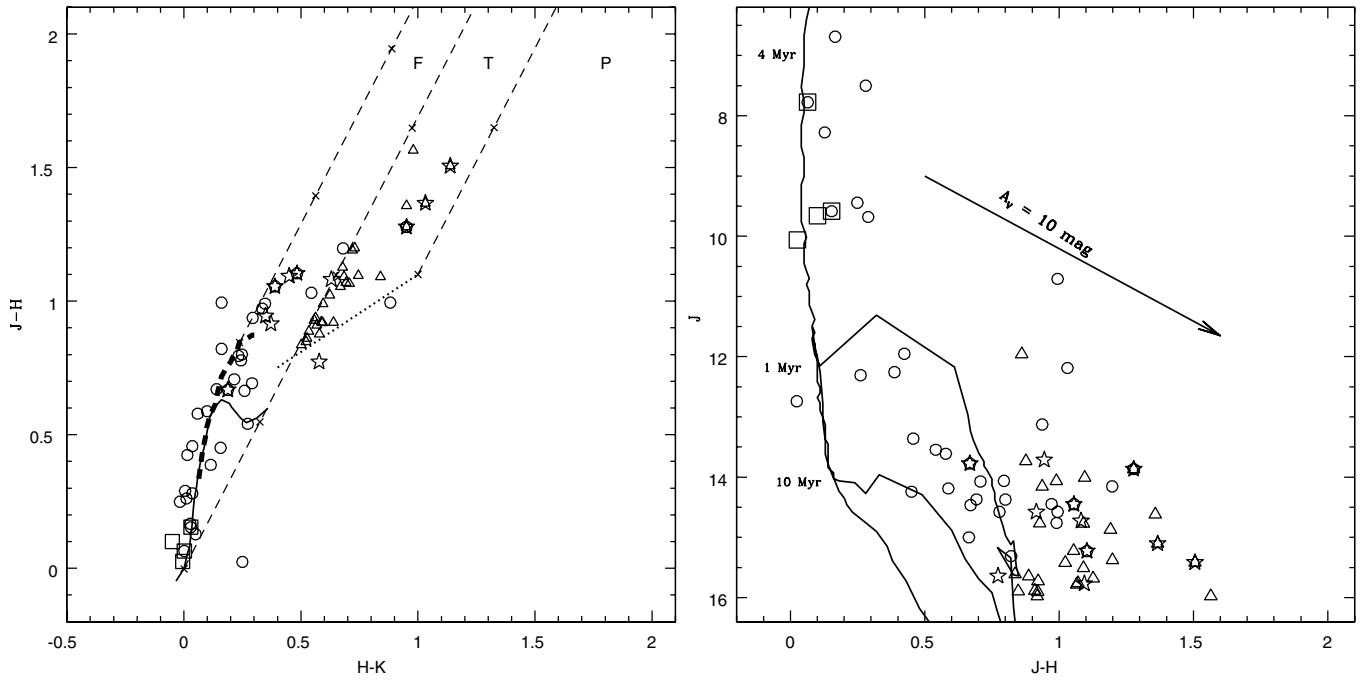

Figure 15. Left: $(J - H)$ vs. $(H - K)$ TCD and (right) J vs. $(J - H)$ CMD for all known YSOs and YSO candidates in the whole region of our study, including O-type stars (squares), Hα stars (asterisks), X-ray stars (open circles), NIR-excess stars as CTTS candidates (triangles), and WTTS candidates (filled circles). The solid curves in the CMD represent the 4 Myr ($Z = 0.02$) main sequence (Bertelli et al. 1994) and PMS isochrones of age 1 and 10 Myr (Siess et al. 2000) appropriate for a distance of 2.57 kpc and a reddening of $A_V = 1.5$ mag.

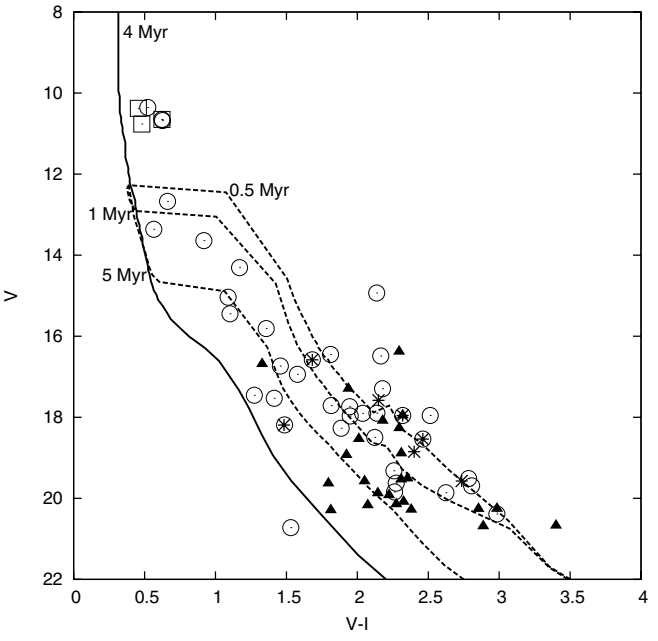

Figure 16. Optical V vs. $(V - I)$ CMD for Hα stars (asterisks), NIR-excess stars (triangles), X-ray stars (open circles), and O-type stars (open squares). Also shown are the isochrone for 4 Myr by Bertelli et al. (1994, solid line) and PMS isochrones for 0.5, 1, and 5 Myr by Siess et al. (2000, dashed lines)—all corrected for a distance of 2.6 kpc and a reddening of $E(B - V) = 0.5$ mag.

incompleteness, we used the ADDSTAR routine as described in Section 2.1. For foreground/background field star contamination, we made use of the Besançon Galactic model of stellar population synthesis (Robin et al. 2003). First, star counts predicted by the Besançon model were found to agree with the observed KLF of an adjacent reference field (Figure 18(a)). The model was applied to the target field to separate the foreground ($d < 2.6$ kpc) and background ($d > 2.6$ kpc) contributions. Toward NGC 7380, the foreground (within 2.6 kpc) extinction was taken to be $A_V \sim 1.55$ mag, whereas the background population (> 2.6 kpc) was simulated with $A_V = 2.2$ mag, from which the fraction of foreground versus background stars was determined and subtracted from the apparent KLF of the cluster to give the intrinsic KLF of the cluster.

The cluster KLF is assumed to follow the form of $dN(K)/dK \propto 10^{\alpha K}$, where $dN(K)/dK$ is the number of stars per 0.5 magnitude bin for magnitude K, and α is the slope of the power law. In the cluster region (Figure 18(b)) $\alpha = 0.31 \pm 0.08$, within the range of $\alpha \sim 0.3$–0.4 typically found for young clusters (Lada et al. 1991; Lada & Lada 1995, 2003). Smaller slopes ($\sim$0.3–0.2) have been reported for some young, embedded clusters (e.g., Megeath et al. 1996; Ojha et al. 2004; Leistra et al. 2005; Sanchawala et al. 2007).

4. DISCUSSION

The reason for the discrepancies in the distances reported in the literature for NGC 7380 is emerging. The OB stars in the region form a part of the Cep OB1 association, whereas the young star cluster occupies only a very small sky area, a few arcminutes across, in this complex region of copious nebulosity and star-forming activities. The largest value of the distance determination, 3.6 kpc by Moffat (1971), was basically suggested to account for the brightness of the DH Cep, as a closer distance would make either component star intrinsically too faint.

DH Cep is an ellipsoidal binary system, i.e., with stellar shape tidally distorted, and has an orbital period of 2.11 days with an inclination angle of $\sim$60° (Pearce 1949). The eclipse has only a 0.05–0.1 mag brightness drop (Lines et al. 1986). The star is too bright in our observations, so we adopted $m_V = 8.58$

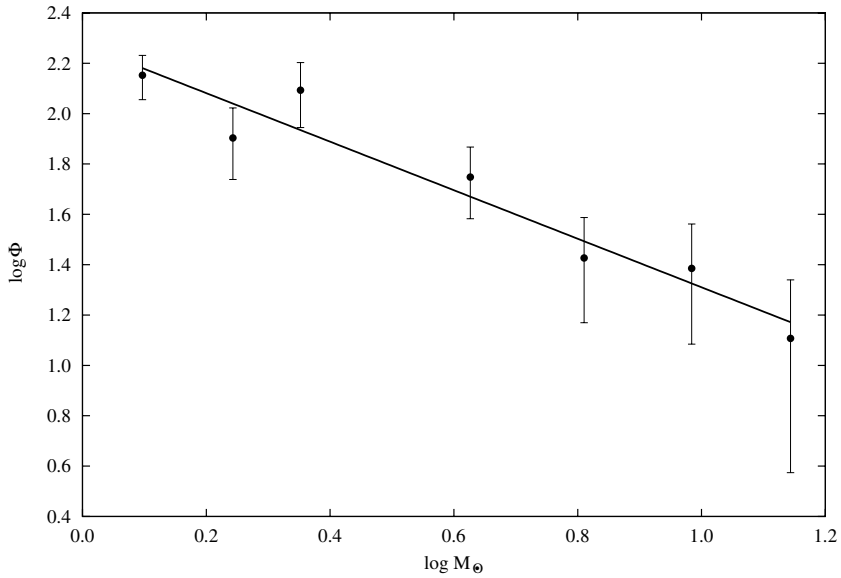

Figure 17. Mass function, $\log\phi = \log N/d\log m$ of NGC 7380. The error bars represent $\pm\sqrt{N}$ errors. The line is the least-squares fit in the mass range $1.0 < M/M_{\odot} < 16.4$.

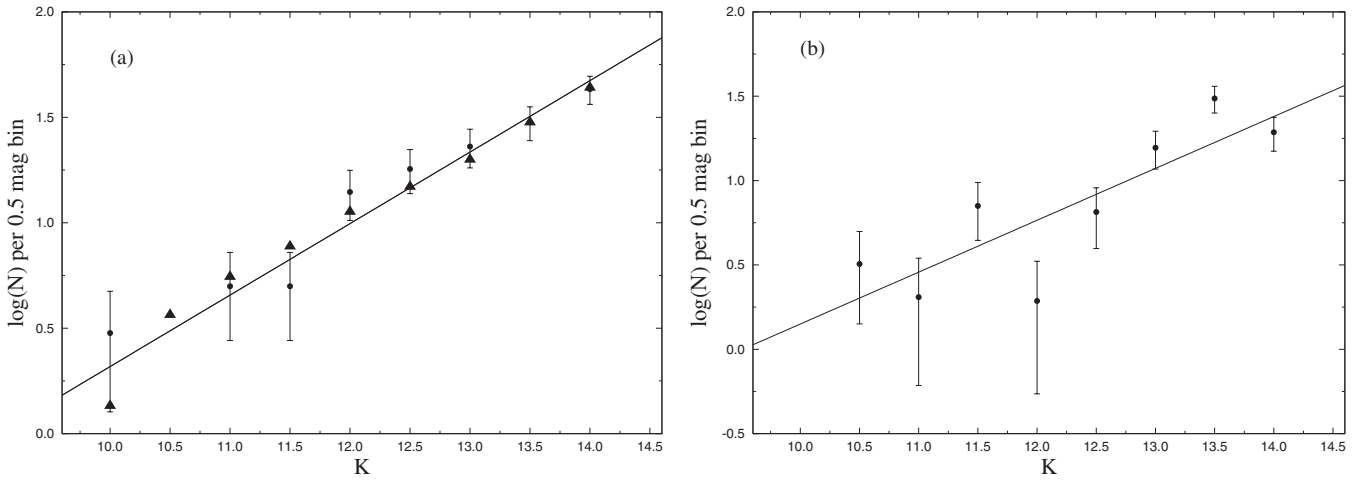

Figure 18. (a) Comparison of the observed (filled circles) and computed (triangles) KLFs of the reference field. Error bars represent $\pm\sqrt{N}$ values. The observed KLF slope α of the reference field (solid line) is 0.36 ± 0.05, comparable to that computed from the Galactic model (Robin et al. 2003) of 0.34 ± 0.02. (b) Corrected KLF for the probable members in the cluster. The line is the least-squares fit, with $\alpha = 0.31 \pm 0.08$, to the data points in the magnitude range 10.5–14.25.

for two identical unresolved stars and an observed $(B - V) = 0.34$ taken from Hoag & Applequist (1965). Now that DH Cep is shown to be associated with NGC 7380, hence at a distance of 2.6 kpc, an absolute magnitude of $M_V = -5.7$, and an intrinsic color of $(B - V)_0 = -0.33$ for an O5/6 star (Schmidt-Kaler 1982), the binary system would have a color excess of $E(B - V) = 0.67$, similar to the cluster value. To account for the apparent magnitude of $m_V = 9.33$ mag of a single star at this distance, then, a visual extinction of ~3.0 is required. This yields a total-to-selective extinction, $R_V \sim 4.4$, higher than the nominal interstellar value of $R_V = 3.1$. A larger R_V value can be attributed to a bigger average grain size (Cardelli et al. 1989; Whittet et al. 2001), and is generally seen toward sources embedded in molecular clouds, where grain growth has occurred, or toward luminous stars in H II regions (Povich et al. 2011; Pandey et al. 2000, e.g.), where smaller grains in the stellar vicinity are more readily evaporated. If DH Cep is such a case of a large R_V value, a longer heliocentric distance suggested by Moffat (1971) is not necessary.

However, as stated earlier, $R_V = 3.1$ was measured toward the rest of the cluster members. This prompts us to search for an alternative to an anomalous R_V value. One possibility is the uncertainty in the absolute magnitudes of very luminous stars. For example, for an O6V, $M_V = -5.7$ (Schmidt-Kaler 1982) or −4.92 (Martins et al. 2005). If a fainter intrinsic brightness for DH Cep is adopted, $m_V = 9.33$ mag, and a distance at 2.6 kpc leads to $A_V = 2.2$, or $R_V = 3.3$, which is close to the nominal value. Stellar binarity and the vertical structure of the upper main sequence make distance determination based on stellar luminosity unreliable. Main-sequence fitting to a sample of photometrically and kinematically confirmed members is preferable in distance and age determinations.

The morphological structure of NGC 7380, with an elongated core and an extended tail, is puzzling. The shape of a star cluster is dictated initially by the condition in the parental molecular cloud. As the cluster evolves, its shape is altered by two-body relaxation arising from encounters among member stars, by stellar evaporation, and by external tidal forces from

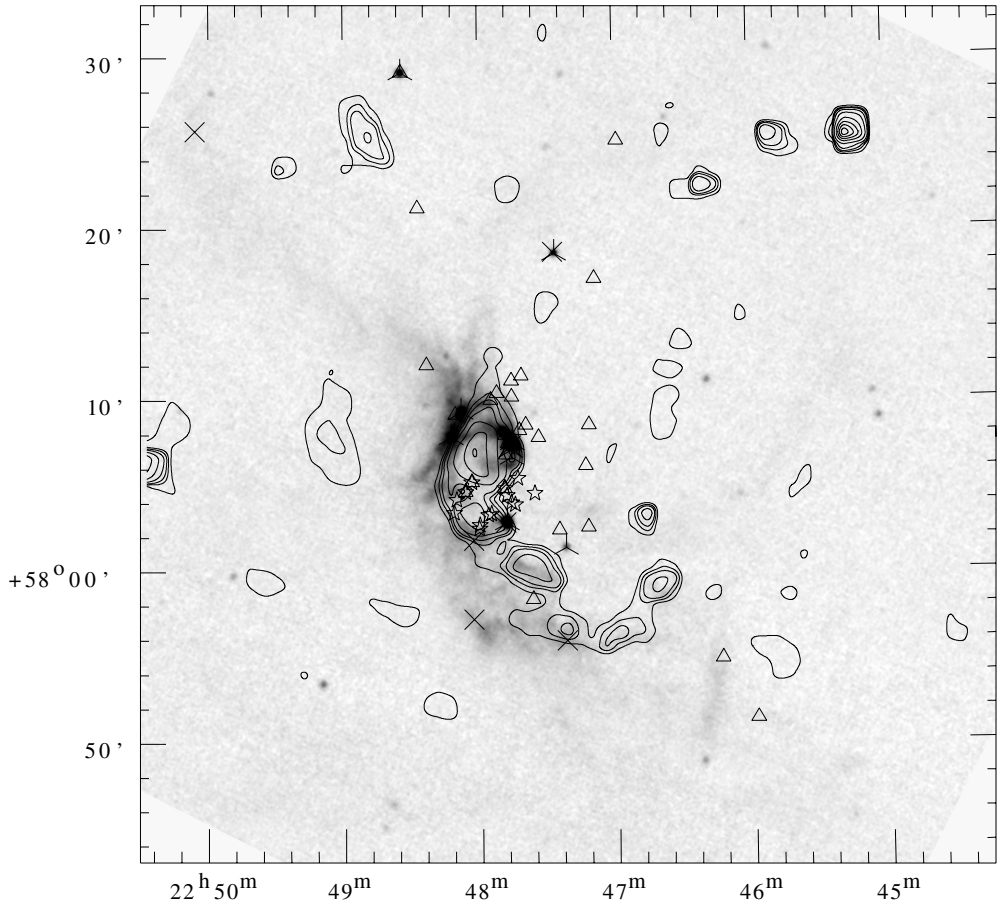

Figure 19. NVSS (1.4 GHz) radio emission, shown as contours at 1%, 2%, 3%, 5%, 10%, 20%, 30%, 40%, 50%, 60%, 70%, 80%, and 90% of the peak value of 0.1613 Jy Beam^{-1}, is superimposed on the *MSX A*-band emission, shown as gray scales. Known YSOs or candidates are marked: IR-excess sources (probable T-Tauri-type stars, open triangles), Hα stars (asterisks), *IRAS* point sources (crosses), *MSX* point sources (three-pointed stars), O-type stars (open squares), and X-ray stars (open circles).

the Galactic disk or a nearby giant molecular cloud (Chen et al. 2004). The shape of NGC 7380 should owe in part to the relic of the original molecular cloud out of which the cluster was formed. As suggested by Moffat (1971), DH Cep is in the final clearing stage of the parental cloud, as evidenced by the low extinction in the cluster region between the illuminating star and the remnant cloud that embraces the cluster. Apparently the ultraviolet radiation from DH Cep has been ionizing the cloud, producing an ionization front that drives a shock into pre-existing cloud clumps, thereby compressing them. They became gravitationally unstable and collapsed to form next-generation stars (Elmegreen 1989, 1998), witnessed as the YSOs in the cloud. The “working layer” is traced as the 1.4 GHz emission by ionized gas, laminating on the surface of the molecular cloud, detected as the *MSX* emission, facing DH Cep, as seen in Figure 19.

Photoevaporation of the molecular cloud by DH Cep is further manifested by cometary globules in the region, each tipped by a young star. Figure 20 shows the Hα image around DH Cep and BRC 43, in which we demonstrate a few examples. Star A is near the bright rim of BRC 43, but saturated in the study by Ogura et al. (2002), so was not listed as an Hα star. Its colors suggest a reddened early-type star. Star B is also at the rim, so the optical photometry has large uncertainties. Its 2MASS colors are consistent with being an early-type star. Another star saturated in the data of Ogura et al. (2002), R.A. = 22:47:47.3, decl. = +58:03:30 (J2000), $V = 12.445$ mag, has colors, $(U - B) = 1.246$, $(B - V) = 1.525$, $(V - I) = 1.621$, $(J - H) = 0.686$, and $(H - Ks) = 0.100$, consistent with being a giant star not associated with the cluster. Star C is at the tip of a dark cometary globule, approximately located in between DH Cep and Star A. Its optical and infrared colors indicate an early-type star with little extinction. Stars D and E are each at the tip of a dark cometary globule pointing away from DH Cep. The optical and infrared colors of Star C suggest a PMS nature, likely a Herbig Ae/Be star. Star E is connected to a prominent cometary nebula, and has colors of an early-type star, either with moderate extinction or slightly above the main sequence. Each of these stars has a proper motion indicative of connection with the cluster (see Table 5), and together with the copious BRCs in the region, likely illuminated and shaped by DH Cep, demonstrating vividly the influence by the luminous star on the remnant molecular clouds.

In addition to the cluster region, which has been a priori recognized as where stellar density is enhanced, many YSOs, particularly mid- and far-infrared sources, are found embedded in the cloud complex to the east, outside of the cluster. Following the same analysis of optical and NIR TCDs presented earlier, these stars have ages in the range of 0.5–1 Myr. Given the uncertainty of PMS evolutionary models at such young ages, the YSOs associated with the clouds therefore seem to be at least the same age as and perhaps even younger than NGC 7380. Many YSOs are away from, and thus not gravitationally bound by, the cluster. Still, they are at the same distance, coeval, and

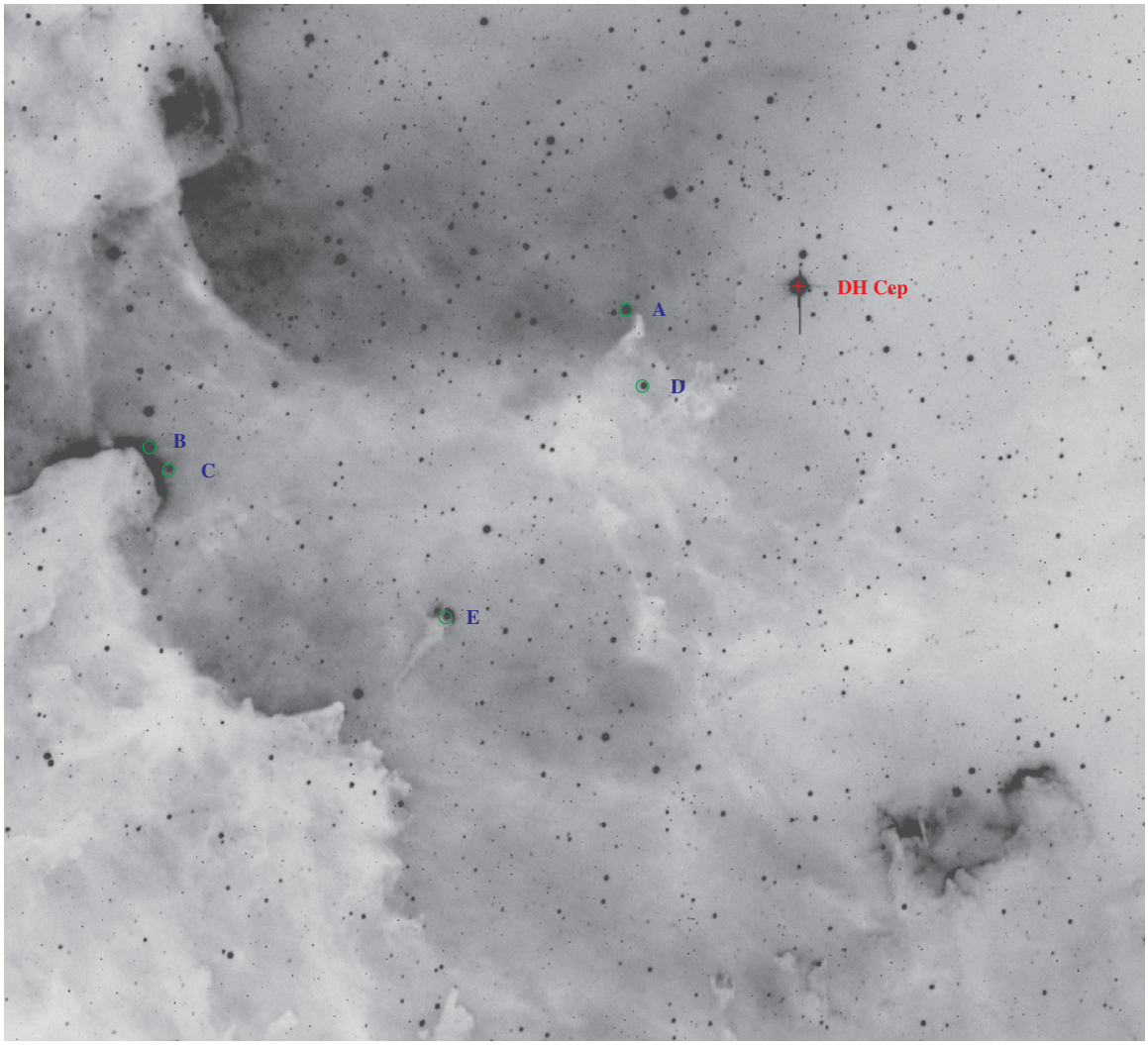

Figure 20. Exposed young stellar objects associated with cometary globules, marked on an Hα image. Note the alignment of these stars with DH Cep and BRCs or globules.

(A color version of this figure is available in the online journal.)

Table 5
Young Stars at the Tip of Cometary Globules

Star	R.A. (2000) Decl. (2000) (h m s ° ′ ″)	V (mag)	$V-I$ (mag)	$U-B$ (mag)	$B-V$ (mag)	J (mag)	$J-H$ (mag)	$H-Ks$ (mag)	μ_α, μ_δ (UCAC3) (mas yr^{-1})
A	22 47 47.13 +58 03 07.3	12.363	0.843	−0.290	0.646	10.930	0.125	0.118	−2.7 (0.8), −2.0 (1.1)
B	22 47 45.48 +58 02 52.4	...	...	...	...	12.297	0.120	0.084	−3.4 (3.2), −4.9 (5.2)
C	22 47 08.28 +58 04 45.2	11.905	0.428	−0.488	0.313	11.093	0.044	0.035	−3.1 (0.8), −3.7 (1.3)
D	22 47 22.40 +58 01 21.5	14.933	2.137	0.441	1.534	10.797	1.034	0.916	−4.5 (6.6), −7.0 (4.9)
E	22 47 06.73 +58 03 55.7	13.144	0.866	−0.004	0.615	11.579	0.210	0.078	−3.2 (0.7), −3.4 (2.4)

comoving with NGC 7380, so likely to have shared the same formation history with the star cluster.

5. SUMMARY

Our photometric and kinematic study of the Galactic open cluster NGC 7380 indicates a distance of 2.6±0.4 kpc, a physical size of ∼6 pc across with an elongated shape plus an extended tail structure, and an age of about 4 Myr. The double O5 star DH Cep, a member of the cluster, is in the final stage to disperse the gas and dust in the cluster region. The young stars outside of the cluster and deeply embedded in molecular clouds are essentially coeval and appear to have formed, perhaps under the influence of DH Cep, after NGC 7380 came into existence.

Part of this work has been carried out under the Taiwan-Indo bilateral collaborative grant NSC 99-2119-M008-021. We acknowledge the support given at Kiso Observatory, Steward Observatory, and Lulin Observatory concerning the data collected for this study. J.S. and W.P.C. acknowledge the Taiwan-Baltic trilateral grant NSC 93-2112-M-008-040 to promote scientific collaboration among Taiwan, Latvia, and Lithuania.

REFERENCES

Baade, D. 1983, A&AS, 51, 235
Baumgardt, H., Dettbarn, C., & Wielen, R. 2000, A&AS, 146, 251
Becker, W., & Fenkart, R. 1971, A&AS, 4, 241
Bertelli, G., Bressan, A., Chiosi, C., Fagotto, F., & Nasi, E. 1994, A&AS, 106, 275
Bessell, M. S., & Brett, J. M. 1988, PASP, 100, 1134
Bhatt, H., Pandey, J. C., Kumar, B., Sagar, R., & Singh, K. P. 2010, New Astron., 15, 755
Cardelli, J. A., Clayton, G. C., & Mathis, J. S. 1989, ApJ, 345, 245
Carraro, G., Vázquez, R. A., Moitinho, A., & Baume, G. 2005, ApJ, 630, L153
Chavarria-K., C., Moreno-Corral, M. A., Hernandez-Toledo, H., Terranegra, L., & de Lara, E. 1994, A&A, 283, 963
Chen, W. P., Chen, C. W., & Shu, C. G. 2004, AJ, 128, 2306
Chini, R., & Wargau, W. F. 1990, A&A, 227, 213
Cohen, J. G., Frogel, J. A., Persson, S. E., & Ellias, J. H. 1981, ApJ, 249, 481
Elmegreen, B. G. 1989, ApJ, 340, 786
Elmegreen, B. G. 1998, in ASP Conf. Ser. 148, Origins, ed. C. E. Woodward, J. M. Shull, & H. A. Thronson (San Francisco, CA: ASP), 150
Georgelin, Y. M., & Georgelin, Y. P. 1976, A&A, 49, 57
Hilditch, R. W., Harries, T. J., & Bell, S. A. 1996, A&A, 314, 165
Hillenbrand, L. A., Strom, S. E., Vrba, F. J., & Keene, J. 1992, ApJ, 397, 613
Hoag, A. A., & Applequist, N. L. 1965, ApJS, 12, 215
Hoag, A. A., Johnson, H. L., Iriarte, B., Mitchell, R. I., Hallam, K. L., & Sharpless, S. 1961, Publ. U.S. Nav. Obs., 17, 347
Johnson, H. L., & Morgan, W. W. 1953, ApJ, 117, 313
Jose, J., et al. 2008, MNRAS, 384, 1675
Jose, J., et al. 2011, MNRAS, 411, 2530
Kharchenko, N. V., et al. 2005, A&A, 438, 1163
Lada, C. J., & Lada, E. A. 2003, ARA&A, 41, 57
Lada, E. A., Evans, N. J., II, Depoy, D. L., & Gatley, I. 1991, ApJ, 371, 171
Lada, E. A., & Lada, C. J. 1995, AJ, 109, 1682
Landolt, A. U. 1992, AJ, 104, 340
Leisawitz, D., Bash, F. N., & Thaddeus, P. 1989, ApJS, 70, 731
Leistra, A., Cotera, A. S., Liebert, J., & Burton, M. 2005, AJ, 130, 1719
Lines, H. C., et al. 1986, IBVS, 2932, 1
Loktin, A. V., & Beshenov, G. V. 2003, Astron. Rep., 47, 6
Martins, F., Schaerer, D., & Hillier, D. J. 2005, A&A, 436, 1049
Massey, P., Johnson, K. E., & Degioia-Eastwood, K. 1995, ApJ, 454, 151
Megeath, S. T., et al. 1996, A&A, 307, 775
Meyer, M., Calvet, N., & Hillenbrand, L. A. 1997, AJ, 114, 288
Moffat, A. F. J. 1971, A&A, 13, 30
Nordström, B., et al. 2004, A&A, 418, 989
Ogura, K., Sugitani, K., & Pickles, A. 2002, AJ, 123, 2597
Ojha, D. K., et al. 2004, ApJ, 616, 1041
Pandey, A. K., Nilakshi, O. K., Sagar, R., & Tarusawa, K. 2001, A&A, 374, 504
Pandey, A. K., Ogura, K., & Sekiguchi, K. 2000, PASJ, 52, 847
Pandey, A. K., Sharma, S., & Ogura, K. 2006, MNRAS, 273, 255
Pandey, A. K., Upadhyay, K., Ogura, K., Sagar, R., Mohan, V., Mito, H., Bhatt, H. C., & Bhatt, B. C. 2005, MNRAS, 358, 1290
Pearce, J. A. 1949, AJ, 54, 135
Penny, L. R., Gies, D. R., & Bagnuolo, W. G., Jr. 1997, ApJ, 483, 439
Perryman, M. A. C., et al. 1997, A&A, 323, 49
Pittard, J. M., & Stevens, I. R. 2002, A&A, 388, L20
Povich, M. S., Townsley, L. K., Broos, P. S., et al. 2011, ApJS, 194, 6
Price, S. D., Egan, M. P., Carey, S. J., Mizuno, D. R., & Kuchar, T. A. 2001, AJ, 121, 2819
Robin, A. C., Reyle, C., Derriere, S., & Picaud, S. 2003, A&A, 409, 523
Robitaille, T. P., Whitney, B. A., Indebetouw, R., Wood, K., & Denzmore, P. 2006, ApJS, 167, 256
Sagar, R., & Richtler, T. 1991, A&A, 250, 324
Salpeter, E. E. 1955, ApJ, 121, 161
Sanchawala, K., et al. 2007, ApJ, 667, 963
Schmidt-Kaler, Th. 1982, in Landolt-Bornstein, Vol. 2b, ed. K. Schaifers, H. H. Voigt, & H. Landolt (Berlin: Springer), 19
Sharpless, S. 1959, ApJS, 4, 257
Siess, L., Dufour, E., & Forestini, M. 2000, A&A, 358, 593
Skrutskie, M. F., et al. 2006, AJ, 131, 1163
Stetson, P. B. 1987, PASP, 99, 191
Sturm, E., & Simon, K. P. 1994, A&A, 282, 93
Tadross, A. L., Werner, P., Osman, A., & Marie, M. 2002, New Astron., 7, 553
Underhill, A. B. 1969, A&A, 1, 356
Upgren, A. R., Sperauskas, J., & Boyle, R. P. 2002, Balt. Astron., 11, 91
Watson, M. G., et al. 2009, A&A, 493, 339
Whittet, D. C. B., Gerakines, P. A., Hough, J. H., & Shenoy, S. S. 2001, ApJ, 547, 872
Zacharias, N., et al. 2010, AJ, 139, 2184
Zhao, J.-L., Chen, L., & Wen, W. 2006, Chin. J. Astron. Astrophys., 6, 435